HHS Public Access

Author manuscript

Neurobiol Aging. Author manuscript; available in PMC 2022 February 01.

Published in final edited form as:

Neurobiol Aging. 2021 February ; 98: 88–98. doi:10.1016/j.neurobiolaging.2020.10.007.

Increased intrinsic excitability and decreased synaptic inhibition in aged somatosensory cortex pyramidal neurons

Ion R. Popescu[a], **Kathy Q. Le**[b], **Alexis L. Ducote**[a,b], **Jennifer E. Li**[b], **Alexandria E. Leland**[b], **Ricardo Mostany**[a,b]

[a]Department of Pharmacology, Tulane University School of Medicine, New Orleans, LA, USA

[b]Tulane Brain Institute, Tulane University, New Orleans, LA, USA

Abstract

Sensorimotor performance declines during advanced age, in part due to deficits in somatosensory acuity. Cortical receptive field expansion is thought to contribute to somatosensory deficits and is suggestive of increased excitability or decreased inhibitory inputs in pyramidal neurons of the primary somatosensory cortex (S1). To ascertain changes in excitability and inhibition, we measured both properties in neurons from vibrissal S1 in brain slices from young and aged mice. Because adapting and non-adapting neurons – the principal pyramidal types in layer 5 (L5) – differ in intrinsic properties and inhibitory inputs, we determined age-dependent changes according to neuron type. We found an age-dependent increase in intrinsic excitability in adapting neurons, caused by a decrease in action potential (AP) threshold. Surprisingly, in non-adapting neurons we found both an increase in excitability caused by increased input resistance, and a decrease

CRediT authorship contribution statement

Ion R. Popescu: Investigation, Conceptualization, Methodology, Software, Validation, Formal analysis, Supervision, Visualization, Funding acquisition, Writing - original draft, Writing – review & editing. **Kathy Q. Le:** Investigation, Conceptualization, Methodology, Software, Formal analysis, Writing – review & editing. **Alexis L. Ducote:** Investigation, Formal analysis, Writing – review & editing. **Jennifer E. Li:** Investigation, Writing – review & editing. **Alexandria E. Leland:** Investigation, Writing – review & editing. **Ricardo Mostany:** Investigation, Conceptualization, Methodology, Software, Validation, Formal Analysis, Supervision, Visualization, Resources, Project administration, Funding acquisition, Writing - original draft, Writing – review & editing.

Disclosure statement

The authors declare no conflicts of interest and no competing financial interests.

Verification

1.

a) None of the authors have any conflicts of interest to declare.

b) The authors' institution has no contracts related to this research which could result in financial gain now or in the future.

c) The authors have no other agreements which could result in financial gain.

2.

This work was funded by NIA/NIH R01AG047296 and Louisiana Board of Regents RCS LEQSF(2016–19)-RD-A-24 to Ricardo Mostany.

3. The data in this manuscript have not been previously published, have not been submitted elsewhere, and will not be submitted elsewhere while under consideration at *Neurobiology of Aging*.

4. All the procedures described in this study were approved by the Institutional Animal Care and Use Committee of Tulane University, and were performed in accordance with the NIH Office of Laboratory Animal Welfare's *Public Health Service Policy on Humane Care and Use of Laboratory Animals and Guide for the Care and Use of Laboratory Animals*.

5. All authors have reviewed the manuscript, approve of its contents and validate the accuracy of the data.

Ion R. Popescu, Kathy Q. Le, Alexis L. Ducote, Jennifer E. Li, Alexandria E. Leland and Ricardo Mostany

in synaptic inhibition. Spike frequency adaptation, already small in non-adapting neurons, was further reduced by aging, whereas sag, a manifestation of I_h, was increased. Therefore, aging caused both a decrease in inhibition and an increase in intrinsic excitability in the murine L5, but these effects were specific to pyramidal neuron type.

Keywords

aging; inhibition; GABA; intrinsic excitability; hyperexcitability; action potential threshold; input resistance; spike frequency adaptation; sag; critical frequency; somatosensory cortex; layer 5; barrel cortex

1. Introduction

A neuron's susceptibilities to aging are biased by its transcriptome, connectivity, and activity patterns. Understanding the aging of the brain, designing prophylaxis and treatment of deteriorating functionality, and in turn understanding the effect of interventions will depend on pinpointing and characterizing age-related changes. For instance, why does advanced age introduce a blunting of sensorimotor function (Bedard et al., 2002; Hermans et al., 2018; Hermans et al., 2019; Heuninckx et al., 2004; Seidler et al., 2010; Serrien et al., 2000; Swinnen, 1998; Wu and Hallett, 2005)? Contributing to sensorimotor changes is the impact of age on the somatosensory system. Sensory acuity declines in primates and rodents (Altun et al., 2007; David-Jurgens et al., 2008; Franco et al., 2015; Kalisch et al., 2009; Porciatti et al., 1999; Shimokata and Kuzuya, 1995; Yoder et al., 2017), and cortical receptive fields expand (David-Jurgens et al., 2008; Fu et al., 2013; Godde et al., 2002; Kalisch et al., 2009; Spengler et al., 1995). Although advanced age introduces both increases (e.g., Simkin et al., 2015) and decreases (e.g., Disterhoft and Oh, 2007) in neuronal excitability, the expansion of cortical receptive fields is most directly explained by increased activation of cortical pyramidal neurons. This is also suggested by the observations that receptive fields are expanded when synaptic inhibition is blocked (Chowdhury and Rasmusson, 2002; Hicks et al., 1986), whereas they are contracted when synaptic inhibition is enhanced (Oka et al., 1986). However, the enlargement of cortical receptive fields in the aged nervous system could also be achieved by increased intrinsic excitability, as suggested by the fact that subthreshold receptive fields are broader than suprathreshold receptive fields (Brecht et al., 2003) and that suprathreshold receptive fields can emerge during postsynaptic depolarization (Lee et al., 2012).

Therefore, we tested for age-related changes in intrinsic excitability and inhibitory synaptic currents in L5 pyramidal neurons of the mouse primary somatosensory cortex barrel field (S1BF) – one of the best understood sensory systems. An important consideration for detecting such changes is that, in both rodents and primates, electrophysiological characteristics are expressed differentially in the two main L5 pyramidal neuron types (Baker et al., 2018; Popescu et al., 2017; for review see Shepherd, 2013). For example, in the S1BF L5 and in the primary motor cortex (M1) L5 of mature young mice spontaneous and miniature inhibitory postsynaptic current (sIPSC and mIPSC) frequencies are significantly lower in adapting pyramidal neurons (also known as thin-tufted or

intratelencephalic) compared to non-adapting pyramidal neurons (also known as thick-tufted or pyramidal tract-type) (Popescu et al., 2017; Ye et al., 2015). Intrinsic properties also differ, i.e., adapting neurons display larger spike frequency adaptation, larger slow afterhyperpolarization (sAHP), longer AP duration, and smaller sag. Conversely, non-adapting neurons display smaller spike frequency adaptation, smaller sAHP, shorter AP duration, and larger sag (Dembrow et al., 2010; Guan et al., 2015; Guan et al., 2018; Hattox and Nelson, 2007; Joshi et al., 2015; Le Be et al., 2007; Oswald et al., 2013; Rock and Apicella, 2015). Therefore, these neuron types may age differently or may undergo similar aging from different baseline values.

We whole cell patch-clamped S1BF L5 pyramidal neurons in brain slices from young and aged mice, and recorded from each neuron intrinsic properties and pharmacologically isolated inhibitory synaptic inputs. We then assigned the neurons to an “adapting” group and a “non-adapting” group using unsupervised clustering methods. Synaptic inhibition and intrinsic properties in adapting and non-adapting neurons were subsequently compared between young and aged mice.

2. Methods

2.1. Animals

We used C57BL/6 (WT) mice provided by NIH-NIA and Tg(Thy-1-EGFP)MJrs/J (GFP-M; Feng et al., 2000) mice bred in-house on the same background (C57BL/6). Data from the two types of mice were pooled. GFP-M mice present with sparse GFP labeling of L5 pyramidal neurons under the thy-1 promoter. Sparsity of GFP expression combined with scarcity of animals over 18 months old rendered data collection from GFP+ neurons inefficient. To overcome this, we obtained C57BL/6 mice from aging-studies colonies maintained by NIH-NIA. Mice were aged 2–6 months (“young”, 30 GFP-M mice) or 18–29 months (“aged”, 11 WT mice and 11 GFP-M mice) at the time of sacrifice. To test for differences between the two strains we compared several age-insensitive parameters (please see Results) - the sAHP, the resting potential (Vm) and the sIPSC amplitude. The sAHP (GFP-M: −1.38 ± 0.11 mV, WT: −1.33 ± 0.13 mV, $p > 0.5$, $n = 65$, 18 cells from 41, 11 mice), Vm (GFP-M: −67.2 ± 0.45 mV, WT: −67.4 ± 0.91 mV, $p > 0.5$, $n = 65$, 18 cells from 41, 11 mice) and sIPSC amplitude (GFP-M: 18.3 ± 1.6 pA, WT: 15.9 ± 1.2 pA, $p > 0.1$, $n = 51$, 15 cells from 37, 11 mice) were not found to be different between the two mouse strains (not shown). We also compared these parameters between the GFP-M aged and WT aged animals. In this case also, the sAHP (GFP-M: −1.24 ± 0.16 mV, WT: −1.33 ± 0.13 mV, $p > 0.5$, $n = 20$, 18 cells from 11, 11 mice), Vm (GFP-M: −65.7 ± 0.72 mV, WT: −67.4 ± 0.91 mV, $p > 0.1$, $n = 20$, 18 from 11, 11 mice) and sIPSC amplitude (GFP-M: 18.0 ± 4.1 pA, WT: 15.9 ± 1.2 pA, $p > 0.5$, $n = 13$, 15 cells from 10, 11 mice) were not found to be different between the two strains (not shown).

Mice were group housed under a 12 h light, 12 h dark cycle, and had access to nesting material as well as food and water *ad libitum*. Experiments were performed during the light hours of the cycle. All the procedures described in this study were approved by the Institutional Animal Care and Use Committee of Tulane University, and were performed in accordance with the NIH Office of Laboratory Animal Welfare’s *Public Health Service*

Policy on Humane Care and Use of Laboratory Animals and Guide for the Care and Use of Laboratory Animals.

2.2. Brain slice preparation.

Mice received general anesthesia by isoflurane inhalation, after which they were decapitated and the brain was quickly removed and submerged in an iced sucrose solution containing (in mM): 234 sucrose, 2.5 KCl, 25 $NaHCO_3$, 1.25 NaH_2PO_4, 7 $MgCl_2$, 0.5 $CaCl_2$, 7 glucose, pH 7.3–7.4, bubbled with 95% O_2, 5% CO_2. After 1–2 min, the brain was blocked in the coronal plane anterior and posterior to the somatosensory cortex. The brain was attached with cyanoacrylate-based glue to a detachable stage, and then sliced in 350 μm increments in the coronal plane on a vibratome (VT 1000 S, Leica Biosystems, Buffalo Grove, NY) while submerged in iced sucrose solution. These coronal brain slices were then incubated 15–30 min at 33 °C in aCSF (in mM): 125 NaCl, 2.5 KCl, 25 $NaHCO_3$, 1.25 NaH_2PO_4, 1 $MgCl_2$, 2 $CaCl_2$, 25 glucose, pH 7.3–7.4, bubbled with 95% O_2, 5% CO_2. Afterwards, slices were maintained for at least one hour at RT in aCSF before being moved to the recording chamber. Slices were allowed to equilibrate for at least 15 min in the recording chamber prior to recording.

2.3 Electrophysiology.

The recording chamber was perfused continuously at a rate of 2 ml/min with aCSF bubbled with 95% O_2, 5% CO_2, and warmed to 29–30 °C. 20 μM 6,7-Dinitroquinoxaline-2,3-dione (DNQX) was included in the aCSF during all recordings. Patch pipettes were pulled in three stages on a horizontal puller (Sutter Instruments, Novato, CA, USA) from borosilicate glass capillaries with ID of 1.2 mm and OD of 1.65 mm (KG-33, King Precision Glass, Claremont, CA, USA). When filled with patch solution (in mM: 70 K-gluconate, 70 KCl, 2 NaCl, 2 $MgCl_2$, 10 HEPES, 1 EGTA, 2 MgATP, 0.3 Na_2GTP, 290 mOsm, pH 7.3 adjusted with KOH) the pipettes had a resistance of 2.5–4.5 MΩ. Pyramidal cells were identified by their distinctive triangular shape and the presence of a clearly visualized apical dendrite extending towards and perpendicular to layer 1. Cells were patch-clamped while visualized with a 40X immersion objective and Dodt gradient contrast in a SliceScope microscope (Scientifica, Uckfield, UK). Recordings were made using a Multiclamp 700B amplifier and a Digidata 1550 digitizer controlled with the Multiclamp Commander program and the pClamp 10 program (Molecular Devices, Sunnyvale, CA, USA). The acquisition frequency was 10 kHz. Voltage clamp traces were Bessel filtered at 2 kHz during acquisition.
The bridge was balanced prior to attempting seal formation. Fast capacitance transients were compensated automatically in Commander after seal formation. Recordings were commenced 2–3 min after break-in and were terminated if the access resistance monitored in the Clampex Membrane Test was ≥ 30 MΩ. Cells with resting membrane potential positive to −60 mV or AP amplitude < 55 mV were excluded from analysis. The input resistance was calculated from 20 pA hyperpolarizing steps. The membrane potential was not adjusted for the liquid junction potential (calculated junction potential = 8.2 mV).

To compute the spike frequency adaptation index (AI), we elicited spikes with a series of 2 s current pulses of amplitude increasing in 5 to 20 pA increments. The index was taken from steps containing 14–16 APs (7–8 Hz). The sAHP was generated with a 70 Hz, 500

ms train of APs, each AP elicited by injecting current via the patch pipette for 5 ms. To study the sag, we delivered a series of 2 s hyperpolarizing pulses from resting potential. The pulse amplitude was increased in 20–40 pA increments and % sag was calculated from steps in which the maximal hyperpolarization was −80 mV to −90 mV. IPSCs were recorded as inward currents at −70 mV. AMPA receptors were blocked throughout our recordings. Thus, intrinsic properties and pharmacologically isolated sIPSCs were recorded from each cell, and excitatory postsynaptic currents (EPSCs) were not recorded in this study.

2.4 Electrophysiology data analysis.

To determine the spike frequency AI, we measured interstimulus intervals (ISIs), excluding the first two. Each ISI was then normalized to the third ISI and plotted as a function of the sequential ISI number. The slope of the linear regression was multiplied by 100 to obtain the AI (Groh et al., 2010; Guan et al., 2015; Popescu et al., 2017). Cells with irregular, stuttering spiking were excluded. Repetitive burst firing was encountered in 11% of cells recorded, and those cells were excluded from further analysis. To determine the sAHP, five consecutive sweeps were averaged and the sAHP was measured at 500 ms after the last AP, relative to the resting membrane potential just before stimulation (Guan et al., 2015). Sag was quantified using the following formula: % sag = 100*(peak change - steady-state change)/(peak change) (Guan et al., 2015). Peak change and steady-state change were measured from the membrane potential just prior to current injection. AP threshold was measured during low frequency spiking generated by 2 s current steps, the first two spikes being excluded, unless otherwise mentioned. The threshold was measured at the time point when the first derivative of the membrane potential (dVm/dt) reached 10 mV/ms (Platkiewicz and Brette, 2010). AP amplitude was measured from threshold to peak. AP duration was measured at half amplitude. Rheobase was the current required to fire at least 3 APs during 2 s sequential depolarizing steps increasing by 10–20 pA. Principal component analysis (PCA) and hierarchical clustering were computed using MATLAB (MathWorks, Natick, MA, USA). Values for sAHP and AP duration at half amplitude from each recording (sample) were scaled (zero mean and unit variance) and centered (subtracting off the mean) before both PCA and pairwise distance between pairs of values were calculated. Singular value decomposition (SVD) algorithm was used to perform PCA. Unsupervised hierarchical clustering was computed using *correlation* as the distance metric and *average* method for linkage of samples. The results from the cluster analysis were further validated using the *clValid* package on R Statistical Software (The R Foundation for Statistical Computing, Vienna, Austria; Version 3.4.1). sIPSCs were detected and measured with MiniAnalysis (Synaptosoft, Fort Lee, NJ, USA), using a detection threshold of 5 pA. The reported IPSC decay time is the time from peak amplitude to 37% of peak amplitude.

2.5 Statistics

Data are provided in text and figures as mean ± SE. Statistical differences between groups were determined using the Student's *t*-test for normally distributed data, and otherwise the Mann-Whitney test. Unpaired two-sample *t*-tests assuming equal variances or assuming unequal variances were used accordingly after applying the *F*-test two-sample for variances in each case. Mixed design two-way repeated measures ANOVA with Bonferroni post hoc

test was used in all comparisons of the AP frequency of young and aged neurons. Statistical significance was set at $p < 0.05$. All p values given are two tailed.

3. Results

3.1. Overall effects of age on L5 pyramidal neurons in S1BF

We initially analyzed the pooled data from all the L5 pyramidal neurons, regardless of their type, to identify age-related differences (Luebke and Chang, 2007; Wong et al., 2000, 2006). The resting membrane potential and AP amplitude were not affected by age (Fig. 1B,C). Thus, there was no apparent age-dependent decline in the viability of recorded neurons. On the other hand, we found that rheobase was significantly lower in the aged group (young: 89.6 ± 4.1 pA, aged: 70.5 ± 4.1 pA, $p < 0.01$, $n = 45, 38$, Fig. 1D) causing neurons from aged mice to fire significantly more APs than those from young mice during near-rheobase current steps (80 pA-young: 3.1 ± 0.6 Hz, aged: 6.9 ± 1.0 Hz, $p < 0.01$; 100 pA-young: 5.9 ± 0.7 Hz, aged: 10.6 ± 1.0 Hz, $p < 0.001$, $n = 45, 38$; not shown). We hypothesized that, since the resting potential was not significantly different, a lower AP threshold or a higher input resistance in the aged neurons were the most likely mechanisms responsible for rheobase reduction. However, neither of these parameters differed by age (Fig. 1E,F), and the cause of rheobase reduction remained to be clarified by further investigation of the different pyramidal neuron types.

We also found that sag, a manifestation of I_h, was increased in aged neurons (young: 18.8 ± 1.0 %, aged: 22.7 ± 1.0 %, $p < 0.01$, $n = 45, 38$, Fig. 1G). On the other hand the sAHP, which plays a role in spike frequency adaptation (Brown and Griffith, 1983; Madison and Nicoll, 1984), was unaffected by age (Fig. 1H,I). Interestingly, this is similar to a report on S1 layer 3 pyramidal neurons (Hickmott and Dinse, 2013), but in contrast with findings in the hippocampus, where it has been shown to be increased in aged pyramidal neurons in CA1 (Gant et al., 2015; Matthews et al., 2009; Tombaugh et al., 2005), but not in CA3 (Oh et al., 2016; Simkin et al., 2015). AP duration also was not affected by age in our recordings (Fig. 1J,K). AP duration and sAHP are active membrane properties known to be differentially expressed in different L5 pyramidal neuron types, and therefore this preliminary analysis signaled them as potential candidates for neuronal classification by cluster analysis (Dembrow et al., 2010; Guan et al., 2015; Guan et al., 2018; Hattox and Nelson, 2007; Joshi et al., 2015; Le Be et al., 2007; Oswald et al., 2013; Popescu et al., 2017; Rock and Apicella, 2015). Finally, AP frequency adaptation was reduced in aged neurons (young: 3.6 ± 1.0, aged: 1.1 ± 0.4, $p < 0.05$, $n = 45, 38$, Fig. 1L).

To further assess age-related changes in excitability we compared the *f-I* relationship in the 160 pA – 280 pA range (starting at ~2 × rheobase). The higher frequency spiking in response to these currents is subject to increased activity-dependent modulation, such as frequency adaptation caused by Ca^{2+}-dependent K^+ currents. The *f-I* relationship showed an age-related increase in excitability (Fig. 1M,N). However, the slope of the linear range of the *f-I* relationship (160 pA – 240 pA) was not different between the age groups, indicating that the increased excitability was not caused by increased gain (Fig 1O).

High frequency (≥ 100 Hz) spikes (HFS) back-propagate efficiently into the apical dendrite in S1 L5 pyramidal neurons from rats and mice *in vivo* (Larkum et al., 1999) and *in vitro* (de Kock and Sakmann, 2008), triggering Ca^{2+} spikes and modulating synaptic integration and plasticity (Beaulieu-Laroche et al., 2019; Nakahata and Yasuda, 2018; Spratt et al., 2019). For this reason, 100 Hz has been named a "critical frequency" in this system. Moreover, modeling work predicts that aging facilitates the ability of HFS to trigger dendritic Ca^{2+} spikes (Coskren et al., 2015). HFS occurring at the onset of depolarization are facilitated by T-type Ca^{2+} currents (Bender et al., 2010; Dumenieu et al., 2018; White et al., 1989), which have been shown to be upregulated in cortical neurons from aged rats (Murchison and Griffith, 1995), possibly due to decreased dopaminergic suppression of T-type Ca^{2+} channel activation (Bender et al., 2010; Jin et al., 2019). We compared the prevalence of HFS-producing neurons from young and aged mice by quantifying HFS during the largest amplitude depolarizing step used (280 pA). We found ISIs ≤ 10 ms only during the first 60 ms (Fig. 1P). Seven out of 45 (15.6%) neurons from young mice exhibited HFS, whereas 14 out of 37 (37.8%) neurons from aged mice did so ($p < 0.05$, chi-square test; Fig. 1Q). Two to three sequential HFS occurred in young cells and two to four in aged cells. Neurons from young mice fired 0.35 ± 0.13 HFS/cell and aged neurons fired 1.1 ± 0.27 HFS/cell during the 2 s step ($p > 0.05$, $n = 45, 37$; not shown). Therefore, there is a higher prevalence of HFS-firing in aged neurons, possibly favoring the generation of Ca^{2+} spikes, which are known to invade dendritic spines (Kwon et al. 2017), potentially contributing to the elevated dendritic spine turnover rates which we have previously reported (Davidson et al., 2020; Mostany et al., 2013; Voglewede et al., 2019).

Finally, we also measured the effect of age on the inhibitory inputs to these pyramidal neurons. The mean frequency of sIPSCs was decreased in aged neurons (young: 14.1 ± 1.5 Hz, aged: 9.6 ± 1.7 Hz, $p < 0.01$, $n = 38, 28$, Fig. 1R). sIPSC amplitude and duration were not different between young and aged neurons (young: 18.4 ± 1.6 pA, 5.2 ± 0.2 ms; aged: 16.9 ± 2.0 pA, 4.9 ± 0.3 ms, $p > 0.05$, $n = 38, 28$; not shown).

3.2. L5 pyramidal neuron classification: adapting vs. non-adapting

We focused our analysis further by assessing the effects of aging on different types of pyramidal neurons. L5 pyramidal neurons' electrophysiological properties co-vary consistently, resulting in two cell groups with contrasting phenotypes of adaptation, sag, sAHP, AP duration, resting potential, and IPSC frequency (Fig. 2). Unsupervised hierarchical cluster analysis on the two active membrane properties unaffected by age, i.e., sAHP and AP duration, yielded two cell groups with profiles conforming closely to those established in the literature and in our previous work (Dembrow et al., 2010; Guan et al., 2015; Guan et al., 2018; Hattox and Nelson, 2007; Joshi et al., 2015; Le Be et al., 2007; Oswald et al., 2013; Popescu et al., 2017; Rock and Apicella, 2015). Thus, cells in the adapting group had larger mean adaptation index, sAHP, AP duration, resting potential, and smaller sag compared to cells in the non-adapting group (AI-adapting: 5.6 ± 1.3, AI-non-adapting: 0.7 ± 0.2, $p < 0.01$; sag-adapting: 15.9 ± 1.1 %, sag-non-adapting: 23.2 ± 0.7 %, $p < 0.001$; sAHP-adapting: −2.2 ± 0.1 mV, sAHP-non-adapting: −0.9 ± 0.04 mV, $p < 0.001$; AP-adapting: 1.0 ± 0.03 ms, AP-non-adapting: 0.8 ± 0.02 ms, $p < 0.001$; Vm-adapting: −69.5 ± 0.6 mV, Vm-non-adapting: −66.0 ± 0.4 mV, $p < 0.001$, $n = 30$

adapting, 53 non-adapting for all metrics, Fig. 2A–F). The prevalence of neurons firing HFS was not different in the two neuron types (9 out of 29 adapting neurons (31%), 10 out of 53 non-adapting neurons (19%), $p > 0.05$, chi-square test; not shown). The mean frequency of sIPSCs was higher in the non-adapting cells (adapting: 7.3 ± 0.9 Hz, non-adapting: 15.2 ± 1.6 Hz, $p < 0.001$, $n = 25, 41$), whereas amplitude and decay time were not different, as found previously (Fig. 2G,H) (Popescu et al., 2017; Ye et al., 2015).

3.3. Effects of aging on adapting neurons

In adapting neurons the resting potential and AP amplitude were not affected by age (Fig. 3A,B). However, rheobase was significantly decreased in aged neurons (young: 86.9 ± 7.3 pA, aged: 61.7 ± 9.9 pA, $p < 0.05$, $n = 18, 12$, Fig. 3C). We asked whether this was caused by an increase in input resistance, but this was not the case (Fig. 3D). Next, we hypothesized that AP threshold was lower in adapting neurons from aged mice. Indeed, the threshold measured during 2 s rheobase pulses (excluding the first two APs) was significantly more negative in neurons from the aged group (young: −41.6 ± 1.0 mV, aged: −46.4 ± 1.4 mV, $p < 0.01$, $n = 18, 12$, Fig. 3E,F). We tested whether the effect of age on threshold was dependent on the duration of the depolarizing step. However, this was not the case, as threshold was also more negative in aged neurons in single spikes elicited with 5 ms intracellular current steps (young: −41.0 ± 0.9 mV; aged: −46.9 ± 1.4 mV, $p < 0.01$, $n = 18, 12$; not shown). These changes suggest an increase in excitability, and are in agreement with the higher frequency of firing measured in aged neurons during near-rheobase current steps (80 pA-young: 3.6 ± 1.1 Hz, aged: 8.8 ± 1.9 Hz, $p > 0.05$; 100 pA-young: 6.3 ± 1.3 Hz, aged: 12.7 ± 2.3 Hz, $p < 0.05$, $n = 18$ young, 12 aged, Fig. 1G).

Sag, sAHP, and AP duration – the latter two used to cluster the adapting and non-adapting groups – were not affected by age in adapting neurons (Fig. 3H-J). However, in aged neurons, we found a trend towards reduced spike frequency adaptation (AI-young: 7.4 ± 2, AI-aged: 2.9 ± 1.0, $p = 0.101$, $n = 18, 12$, Fig. 3K). The *f-I* relationship suggested qualitatively an age-related increase in AP generation that was not statistically significant (Fig. 3L,M). Finally, we found no differences in IPSC frequency, amplitude, or duration between adapting neurons from young and aged mice (Fig. 3N–P).

3.4. Effect of aging on non-adapting neurons

In non-adapting neurons, as in adapting neurons, the membrane resting potential and AP amplitude were not affected by age (Fig. 4A,B). On the other hand, we found an age-dependent reduction in rheobase, as had also been the case for adapting neurons (young: 91.3 ± 4.9 pA, aged: 74.6 ± 5.5 pA, $p < 0.05$, $n = 27, 26$, Fig. 4C). In keeping with this, near-rheobase AP frequency was increased in the neurons from aged mice (80 pA-young: 2.9 ± 0.7 Hz, aged: 6.1 ± 1.1 Hz, $p < 0.05$; 100 pA-young: 5.7 ± 0.8, aged: 9.7 ± 1.1 Hz, $p < 0.01$, $n = 27$ young, 26 aged, Fig. 4D). We asked whether the change in rheobase and in near-rheobase spiking was due to a difference in spike threshold between the two age groups, but this was not the case in non-adapting neurons (Fig. 4E). Another important mechanism determining rheobase and excitability is the input resistance. Therefore, we compared the input resistance of non-adapting neurons, and found that it was higher in the aged group (young: 115.6 ± 6.0 MΩ, aged: 144.6 ± 11.8 pA, $p < 0.05$, $n = 27, 26$, Fig. 4F).

As in adapting neurons, sAHP and AP duration at half-amplitude were not different in the two age groups (Fig. 4G,H). We also measured sag, a consequence of I_h, which endows the neuronal membrane with electrical resonance (Dembrow et al., 2010; Luthi et al., 1998) and narrows the time window of postsynaptic potential summation in dendrites (Harnett et al., 2015; Magee, 1999). We found a robust age-linked increase in % sag (young: 21.3 ± 1.0 %, aged: 25.2 ± 0.9 %, $p < 0.01$, $n = 27, 26$, Fig. 4I,J). The mean AI, already small in young neurons of this subtype, was further decreased in aged neurons (young: 1.1 ± 0.3, aged: 0.3 ± 0.2, $p < 0.05$, $n = 27, 26$, Fig. 4K,L). We hypothesized that blunting of spiking-dependent threshold increase could account for the lowered AI (Higgs and Spain, 2011). However, the increase in threshold from AP1 to AP35 in a 70 Hz, 500 ms train did not differ with age (young: 2.5 ± 0.3 mV, aged: 2.4 ± 0.3 mV, $p > 0.05$, $n = 27, 26$; not shown).

When we examined the *f-I* relationships of non-adapting neurons we found an age-related increase in frequency (Fig. 4M,N). However, gain was not affected by age (young, 0.1 ± 0.005 Hz/pA; aged, 0.1 ± 0.006 Hz/pA, $p > 0.05$, $n = 27, 26$; not shown). We also asked whether the age-related increase in the *f-I* function was entirely due to the decrease in rheobase. Therefore, we replotted the *f-I* function after we subtracted the rheobase from the X-values (Fig. 4O). The fact that the resulting curves are not superimposed suggests that the difference in rheobase is not solely responsible for the leftward shift of the *f-I* function in the neurons from aged animals. Finally, in non-adapting neurons the increased excitability was accompanied by reduced inhibition – the sIPSC frequency was significantly lower in aged neurons (young: 18.5 ± 2 Hz, aged: 11.0 ± 2.4 Hz, $p < 0.001$, $n = 23, 18$), while sIPSC amplitude and decay time were not affected (Fig. 4P,Q).

4. Discussion

L5 generates the primary output stream of the neocortical column, and the two pyramidal types in L5 display a well-characterized dichotomy for an array of electrophysiological characteristics. Recent work suggests that sensory stimulus selectivity, behavioral function, and contribution to pathology may also be differentially distributed (Kim et al., 2015; Lur et al., 2016; Shepherd, 2013; Tang and Higley, 2020). For example, non-adapting neurons in primary visual cortex L5 are thought to be more likely to provide output that informs movement control (Kim et al., 2015), and, unlike adapting neurons, they contribute to eyeblink conditioning (Tang and Higley, 2020). Adapting neurons, on the other hand, are thought to provide a more prominent contribution to visual perception (Kim et al., 2015). Therefore, we wanted to record from the two L5 pyramidal neuron types in the mouse in order obtain an index of age-related changes in the neurons' physiology, and to better understand how aging affects cortical sensory function.

We distinguished pyramidal types by their active properties. Among the active properties documented to co-vary within and differ between the two types only sAHP and AP duration were unaffected by age in our analysis of pooled L5 neurons. Therefore, types were assigned according to PCA/cluster analysis of sAHP and AP duration. The resulting clusters, dubbed "adapting" and "non-adapting," conformed well to the established profile of intrinsic properties and IPSC frequency, and also confirmed the age-independent nature of the sAHP amplitude and the AP duration in S1BF L5 pyramidal neurons (Dembrow et al., 2010; Guan

et al., 2015; Guan et al., 2018; Joshi et al., 2015; Le Be et al., 2007; Oswald et al., 2013; Popescu et al., 2017; Rock and Apicella, 2015). HFS-exhibiting neurons were not differently distributed in the two neuron types, as has also been found in S1BF L5 *in vivo* recordings (de Kock et al., 2007). The age-related changes seen in pooled L5 pyramidal neurons included higher excitability (Fig. 1D,M,N), a larger preponderance of cells displaying HFS (Fig. 1P,Q), lower AP frequency adaptation (Fig. 1L), higher sag (Fig. 1G), and lower IPSC frequency (Fig. 1R). However, when adapting and non-adapting neurons were considered separately, a picture of differential aging emerged.

In adapting neurons, we found a decrease in rheobase, resulting in increased spiking during near-rheobase current steps. Low frequency activity is relevant since *in vivo* spontaneous and whisker-evoked spiking in adapting neurons is also low frequency (de Kock et al., 2007). The mechanism likely underlying the decreased rheobase was the lowered AP threshold. Threshold is determined largely by voltage-gated channels and by the morphology of the axon initial segment (Ding et al., 2018). An increase in the $Na_V1.6$ to $Na_V1.2$ ratio occurring during development in the axon initial segment lowers the AP threshold (Bender et al., 2010; Kole and Stuart, 2012). It would be of interest to determine whether a further change in this ratio occurs in advanced age. Alterations in neuromodulation could also affect the AP threshold – for example decreased dopamine D2-family receptor binding causing increased activation of low-voltage-activated Ca^{2+} channels, thereby lowering the AP threshold (Bender et al., 2010; Jin et al., 2019; Kole and Stuart, 2012). Interestingly, decreased dopaminergic function may also underlie altered decision making in aged animals (Burwell et al., 1995; Simon et al., 2010). We also found a trend ($p = 0.101$) towards decreased spike frequency adaptation, potentially caused by the lower AP threshold (Higgs and Spain, 2011). The *f-I* function was not significantly affected by age, in spite of the lowered rheobase. This probably stems from the high variance of firing frequencies in adapting neurons (Fig. 3L,M). We posit that these neurons have a wide range of spike frequency adaptation and of sAHP, which would affect the AP frequency but not the rheobase.

In non-adapting neurons, we also found a reduction in rheobase, but the underlying mechanism was an increase in input resistance instead of a decrease in AP threshold. Modeling work predicts that decreased dendritic arborization may contribute to increased input resistance in aged neurons (Kabaso et al., 2009). Decreased $GABA_AR$ opening is also a potential mechanism of increased input resistance in the non-adapting neurons from aged mice. *In vivo* spontaneous and whisker-evoked spiking is largely low frequency in this neuronal type also, suggesting that the increase in near-rheobase excitability is physiologically relevant (de Kock et al., 2007; de Kock and Sakmann, 2008).

Non-adapting (i.e., minimally-adapting) neurons displayed a further reduction in adaptation during aging, similar to rat lumbar motoneurons (Kalmar et al., 2009), but unlike rat hippocampal CA1 pyramidal neurons, in which adaptation increased (Disterhoft and Oh, 2007). The decrease here was not caused by a decrease of the sAHP or a blunting of spike-dependent threshold adaptation. Spike frequency adaptation is an ubiquitous phenomenon supported by a variety of mechanism. Other contributors to adaptation that could be affected by aging include the non-inactivating potassium current I_M (Benda and Herz, 2003; Brown

and Adams, 1980) and the slow delayed rectifier-generated potassium current $I(K_S)$ (Dubois, 1981; Schwarz et al., 2006). The most direct implications of diminished adaptation are a decrease in high-pass filtering ability (Higgs and Spain, 2011) and in the precision of temporal coding (Benda et al., 2005). It is also a potential contributor to the leftward-shift in the *f-I* function of neurons from aged mice.

Aging entailed an increase in sag, as also found in cochlear neurons (Shen et al., 2018) and M1 L5 pyramidal neurons (Buskila et al., 2019). Sag is a manifestation of I_h, whose influence on excitability is equivocal (Gasparini and DiFrancesco, 1997; Ko et al., 2016; Shen et al., 2018; Sun et al., 2003). However, the importance of I_h in sharpening postsynaptic potential coincidence detection means that it will be of particular interest to determine if aging also increases I_h in dendrites (Harnett et al., 2015; Magee, 1999).

IPSC frequency was lower in neurons from aged mice. We have found that S1BF L5 pyramidal neuron IPSC frequency is activity-independent in brain slices (Popescu et al., 2017). Therefore, the reduction in IPSC frequency reflects minis and was due to decreased spontaneous release or a reduction in synapse number. Decreased probability of GABA release has been found at synapses on S1BF layer 2/3 pyramidal neurons in aged rats (Hickmott and Dinse, 2013), and declines in the number of inhibitory synapses have also been reported (Luebke et al., 2015; Majdi et al., 2007; Peters et al., 2008). Sensory processing in S1BF utilizes a sparse coding strategy dependent on short latency IPSCs in L5 pyramidal neurons (Petersen, 2019). Sparse coding would be undermined directly by a decrease in sensory stimulus-timed synaptic inhibition, and indirectly by the reduction in $GABA_AR$-generated shunting and the resulting increase in excitability. When synaptic inhibition is weakened, HFS backpropagation into the apical dendrites is also more likely to trigger Ca^{2+} spikes (de Kock and Sakmann, 2008) altering sensory processing and actin dynamics in dendritic spines (Nakahata and Yasuda, 2018). The decline in inhibitory function has been documented in the hippocampus also (Haberman et al., 2011; Potier et al., 2006; Potier et al., 1992; Spiegel et al., 2013), although in contrast to the prefrontal cortex (Banuelos et al., 2013; Bories et al., 2013; Luebke et al., 2004), and may contribute to the reduction in gamma band activity reported in aged mice (Cardin et al., 2009; Jessen et al., 2017).

Finally, our results suggest the hypothesis that homeostatic control is deficient in aged L5 pyramidal neurons (Radulescu et al., 2019; Turrigiano, 2017). Homeostatic mechanisms would be expected to counter increased intrinsic excitability with increased synaptic inhibition (Peng et al., 2010) or, conversely, to counter decreased synaptic inhibition with decreased intrinsic excitability (Turrigiano et al., 1998). Therefore, the co-occurrence of increased excitability and decreased inhibition in the aged mice is suggestive of dysregulated homeostatic regulation and a potential direction of future research.

5. Conclusion

In this study we found evidence supporting the hypothesis of heightened excitability and lowered inhibition in the primary somatosensory cortex during advanced age. However, these changes, and some of their underlying mechanisms, were not uniformly exhibited

in the two types of L5 principal neurons. As mentioned in the introduction, we view the pinpointing of age-related changes in neuronal physiology as a step towards designing treatments and interpreting their effects. It is currently still challenging to target specific neuronal types with anti-aging interventions. However, increasing the resolution of our elucidation of aging to the level of specific neuron types could enable us to better interpret the effects of currently attempted interventions. As an example, the testing of modafinil as a cognitive enhancer in the elderly (Battleday and Brem, 2015; Punzi et al., 2017) can now be considered in the context of dopamine-induced increase of AP threshold (Bender et al., 2010; Jin et al., 2019). We would not have been able to propose this mechanism had we limited our analysis to pooled neurons, which did not reveal the age-related decrease in AP threshold that we found to be specific to adapting neurons.

Acknowledgments

We would like to acknowledge the following for research funding: NIA/NIH R01AG047296 and Louisiana Board of Regents RCS LEQSF(2016–19)-RD-A-24 to RM. We would like to thank Dr. Jeffrey G. Tasker, Dr. Laura A. Schrader and Dr. Rebecca E. Green for their expert opinions during consultations about this work. We would also like to thank Hernán Mejía-Gómez, Anushka Ghosh and Dan Liu for valuable technical assistance.

References

Altun M, Bergman E, Edstrom E, Johnson H, Ulfhake B, 2007. Behavioral impairments of the aging rat. Physiol Behav92(5), 911–923. [PubMed: 17675121]

Baker A, Kalmbach B, Morishima M, Kim J, Juavinett A, Li N, Dembrow N, 2018. Specialized subpopulations of deep-layer pyramidal neurons in the neocortex: Bridging cellular properties to functional consequences. J Neurosci38(24), 5441–5455. [PubMed: 29798890]

Banuelos C, LaSarge CL, McQuail JA, Hartman JJ, Gilbert RJ, Ormerod BK, Bizon JL, 2013. Age-related changes in rostral basal forebrain cholinergic and gabaergic projection neurons: Relationship with spatial impairment. Neurobiol Aging34(3), 845–862. [PubMed: 22817834]

Battleday RM, Brem AK, 2015. Modafinil for cognitive neuroenhancement in healthy non-sleep-deprived subjects: A systematic review. Eur Neuropsychopharmacol25(11), 1865–1881. [PubMed: 26381811]

Beaulieu-Laroche L, Toloza EHS, Brown NJ, Harnett MT, 2019. Widespread and highly correlated somato-dendritic activity in cortical layer 5 neurons. Neuron103(2), 235–241 e234. [PubMed: 31178115]

Bedard AC, Nichols S, Barbosa JA, Schachar R, Logan GD, Tannock R, 2002. The development of selective inhibitory control across the life span. Dev Neuropsychol21(1), 93–111. [PubMed: 12058837]

Benda J, Herz AV, 2003. A universal model for spike-frequency adaptation. Neural Comput15(11), 2523–2564. [PubMed: 14577853]

Benda J, Longtin A, Maler L, 2005. Spike-frequency adaptation separates transient communication signals from background oscillations. J Neurosci25(9), 2312–2321. [PubMed: 15745957]

Bender KJ, Ford CP, Trussell LO, 2010. Dopaminergic modulation of axon initial segment calcium channels regulates action potential initiation. Neuron68(3), 500–511. [PubMed: 21040850]

Bories C, Husson Z, Guitton MJ, De Koninck Y, 2013. Differential balance of prefrontal synaptic activity in successful versus unsuccessful cognitive aging. J Neurosci33(4), 1344–1356. [PubMed: 23345211]

Brecht M, Roth A, Sakmann B, 2003. Dynamic receptive fields of reconstructed pyramidal cells in layers 3 and 2 of rat somatosensory barrel cortex. J Physiol553(Pt 1), 243–265. [PubMed: 12949232]

Brown DA, Adams PR, 1980. Muscarinic suppression of a novel voltage-sensitive K^+ current in a vertebrate neurone. Nature283(5748), 673–676. [PubMed: 6965523]

Brown DA, Griffith WH, 1983. Calcium-activated outward current in voltage-clamped hippocampal neurones of the guinea-pig. J Physiol337, 287–301. [PubMed: 6875931]

Burwell RD, Lawler CP, Gallagher M, 1995. Mesostriatal dopamine markers in aged long-evans rats with sensorimotor impairment. Neurobiol Aging16(2), 175–186. [PubMed: 7777135]

Buskila Y, Kekesi O, Bellot-Saez A, Seah W, Berg T, Trpceski M, Yerbury JJ, Ooi L, 2019. Dynamic interplay between h-current and m-current controls motoneuron hyperexcitability in amyotrophic lateral sclerosis. Cell Death Dis10(4), 310. [PubMed: 30952836]

Cardin JA, Carlen M, Meletis K, Knoblich U, Zhang F, Deisseroth K, Tsai LH, Moore CI, 2009. Driving fast-spiking cells induces gamma rhythm and controls sensory responses. Nature459(7247), 663–667. [PubMed: 19396156]

Chowdhury SA, Rasmusson DD, 2002. Comparison of receptive field expansion produced by GABA(B) and GABA(A) receptor antagonists in raccoon primary somatosensory cortex. Exp Brain Res144(1), 114–121. [PubMed: 11976765]

Coskren PJ, Luebke JI, Kabaso D, Wearne SL, Yadav A, Rumbell T, Hof PR, Weaver CM, 2015. Functional consequences of age-related morphologic changes to pyramidal neurons of the rhesus monkey prefrontal cortex. J Comput Neurosci38(2), 263–283. [PubMed: 25527184]

David-Jurgens M, Churs L, Berkefeld T, Zepka RF, Dinse HR, 2008. Differential effects of aging on fore- and hindpaw maps of rat somatosensory cortex. PLoS One3(10), e3399. [PubMed: 18852896]

Davidson AM, Mejia-Gomez H, Jacobowitz M, Mostany R, 2020. Dendritic spine density and dynamics of layer 5 pyramidal neurons of the primary motor cortex are elevated with aging. Cereb Cortex30(2), 767–777. [PubMed: 31298696]

de Kock CP, Bruno RM, Spors H, Sakmann B, 2007. Layer- and cell-type-specific suprathreshold stimulus representation in rat primary somatosensory cortex. J Physiol581(Pt 1), 139–154. [PubMed: 17317752]

de Kock CP, Sakmann B, 2008. High frequency action potential bursts (≥ 100 hz) in l2/3 and l5b thick tufted neurons in anaesthetized and awake rat primary somatosensory cortex. J Physiol586(14), 3353–3364. [PubMed: 18483066]

Dembrow NC, Chitwood RA, Johnston D, 2010. Projection-specific neuromodulation of medial prefrontal cortex neurons. J Neurosci30(50), 16922–16937. [PubMed: 21159963]

Ding Y, Chen T, Wang Q, Yuan Y, Hua T, 2018. Axon initial segment plasticity accompanies enhanced excitation of visual cortical neurons in aged rats. Neuroreport29(18), 1537–1543. [PubMed: 30320703]

Disterhoft JF, Oh MM, 2007. Alterations in intrinsic neuronal excitability during normal aging. Aging Cell6(3), 327–336. [PubMed: 17517042]

Dubois JM, 1981. Evidence for the existence of three types of potassium channels in the frog Ranvier node membrane. J Physiol318, 297–316. [PubMed: 6275068]

Dumenieu M, Senkov O, Mironov A, Bourinet E, Kreutz MR, Dityatev A, Heine M, Bikbaev A, Lopez-Rojas J, 2018. The low-threshold calcium channel Cav3.2 mediates burst firing of mature dentate granule cells. Cereb Cortex28(7), 2594–2609. [PubMed: 29790938]

Feng G, Mellor RH, Bernstein M, Keller-Peck C, Nguyen QT, Wallace M, Nerbonne JM, Lichtman JW, Sanes JR, 2000. Imaging neuronal subsets in transgenic mice expressing multiple spectral variants of gfp. Neuron28(1), 41–51. [PubMed: 11086982]

Franco PG, Santos KB, Rodacki AL, 2015. Joint positioning sense, perceived force level and two-point discrimination tests of young and active elderly adults. Braz J Phys Ther19(4), 304–310. [PubMed: 26443978]

Fu Y, Yu S, Ma Y, Wang Y, Zhou Y, 2013. Functional degradation of the primary visual cortex during early senescence in rhesus monkeys. Cereb Cortex23(12), 2923–2931. [PubMed: 22941715]

Gant JC, Chen KC, Kadish I, Blalock EM, Thibault O, Porter NM, Landfield PW, 2015. Reversal of aging-related neuronal Ca^{2+} dysregulation and cognitive impairment by delivery of a transgene encoding FK506-binding protein 12.6/1b to the hippocampus. J Neurosci35(30), 10878–10887. [PubMed: 26224869]

Gasparini S, DiFrancesco D, 1997. Action of the hyperpolarization-activated current (ih) blocker ZD 7288 in hippocampal CA1 neurons. Pflugers Arch435(1), 99–106. [PubMed: 9359908]

Godde B, Berkefeld T, David-Jurgens M, Dinse HR, 2002. Age-related changes in primary somatosensory cortex of rats: Evidence for parallel degenerative and plastic-adaptive processes. Neurosci Biobehav Rev26(7), 743–752. [PubMed: 12470685]

Groh A, Meyer HS, Schmidt EF, Heintz N, Sakmann B, Krieger P, 2010. Cell-type specific properties of pyramidal neurons in neocortex underlying a layout that is modifiable depending on the cortical area. Cereb Cortex20(4), 826–836. [PubMed: 19643810]

Guan D, Armstrong WE, Foehring RC, 2015. Electrophysiological properties of genetically identified subtypes of layer 5 neocortical pyramidal neurons: Ca^{2+} dependence and differential modulation by norepinephrine. J Neurophysiol113(7), 2014–2032. [PubMed: 25568159]

Guan D, Pathak D, Foehring RC, 2018. Functional roles of Kv1-mediated currents in genetically identified subtypes of pyramidal neurons in layer 5 of mouse somatosensory cortex. J Neurophysiol120(2), 394–408. [PubMed: 29641306]

Haberman RP, Colantuoni C, Stocker AM, Schmidt AC, Pedersen JT, Gallagher M, 2011. Prominent hippocampal CA3 gene expression profile in neurocognitive aging. Neurobiol Aging32(9), 1678–1692. [PubMed: 19913943]

Harnett MT, Magee JC, Williams SR, 2015. Distribution and function of HCN channels in the apical dendritic tuft of neocortical pyramidal neurons. J Neurosci35(3), 1024–1037. [PubMed: 25609619]

Hattox AM, Nelson SB, 2007. Layer V neurons in mouse cortex projecting to different targets have distinct physiological properties. J Neurophysiol98(6), 3330–3340. [PubMed: 17898147]

Hermans L, Leunissen I, Pauwels L, Cuypers K, Peeters R, Puts NAJ, Edden RAE, Swinnen SP, 2018. Brain gaba levels are associated with inhibitory control deficits in older adults. J Neurosci38(36), 7844–7851. [PubMed: 30064995]

Hermans L, Maes C, Pauwels L, Cuypers K, Heise KF, Swinnen SP, Leunissen I, 2019. Age-related alterations in the modulation of intracortical inhibition during stopping of actions. Aging (Albany NY)11(2), 371–385. [PubMed: 30670675]

Heuninckx S, Debaere F, Wenderoth N, Verschueren S, Swinnen SP, 2004. Ipsilateral coordination deficits and central processing requirements associated with coordination as a function of aging. J Gerontol B Psychol Sci Soc Sci59(5), P225–232. [PubMed: 15358795]

Hickmott P, Dinse H, 2013. Effects of aging on properties of the local circuit in rat primary somatosensory cortex (S1) in vitro. Cereb Cortex23(10), 2500–2513. [PubMed: 22879353]

Hicks TP, Metherate R, Landry P, Dykes RW, 1986. Bicuculline-induced alterations of response properties in functionally identified ventroposterior thalamic neurones. Exp Brain Res63(2), 248–264. [PubMed: 3758246]

Higgs MH, Spain WJ, 2011. Kv1 channels control spike threshold dynamics and spike timing in cortical pyramidal neurones. J Physiol589(Pt 21), 5125–5142. [PubMed: 21911608]

Jessen SB, Mathiesen C, Lind BL, Lauritzen M, 2017. Interneuron deficit associates attenuated network synchronization to mismatch of energy supply and demand in aging mouse brains. Cereb Cortex27(1), 646–659. [PubMed: 26514162]

Jin X, Chen Q, Song Y, Zheng J, Xiao K, Shao S, Fu Z, Yi M, Yang Y, Huang Z, 2019. Dopamine D2 receptors regulate the action potential threshold by modulating T-type calcium channels in stellate cells of the medial entorhinal cortex. J Physiol597(13), 3363–3387. [PubMed: 31049961]

Joshi A, Middleton JW, Anderson CT, Borges K, Suter BA, Shepherd GM, Tzounopoulos T, 2015. Cell-specific activity-dependent fractionation of layer 2/3-->5b excitatory signaling in mouse auditory cortex. J Neurosci35(7), 3112–3123. [PubMed: 25698747]

Kabaso D, Coskren PJ, Henry BI, Hof PR, Wearne SL, 2009. The electrotonic structure of pyramidal neurons contributing to prefrontal cortical circuits in macaque monkeys is significantly altered in aging. Cereb Cortex19(10), 2248–2268. [PubMed: 19150923]

Kalisch T, Ragert P, Schwenkreis P, Dinse HR, Tegenthoff M, 2009. Impaired tactile acuity in old age is accompanied by enlarged hand representations in somatosensory cortex. Cereb Cortex19(7), 1530–1538. [PubMed: 19008462]

Kalmar JM, Button DC, Gardiner K, Cahill F, Gardiner PF, 2009. Caloric restriction does not offset age-associated changes in the biophysical properties of motoneurons. J Neurophysiol101(2), 548–557. [PubMed: 18784275]

Kim EJ, Juavinett AL, Kyubwa EM, Jacobs MW, Callaway EM, 2015. Three types of cortical layer 5 neurons that differ in brain-wide connectivity and function. Neuron88(6), 1253–1267. [PubMed: 26671462]

Ko KW, Rasband MN, Meseguer V, Kramer RH, Golding NL, 2016. Serotonin modulates spike probability in the axon initial segment through HCN channels. Nat Neurosci19(6), 826–834. [PubMed: 27110919]

Kole MH, Stuart GJ, 2012. Signal processing in the axon initial segment. Neuron73(2), 235–247. [PubMed: 22284179]

Larkum ME, Kaiser KM, Sakmann B, 1999. Calcium electrogenesis in distal apical dendrites of layer 5 pyramidal cells at a critical frequency of back-propagating action potentials. Proc Natl Acad Sci U S A96(25), 14600–14604. [PubMed: 10588751]

Le Be JV, Silberberg G, Wang Y, Markram H, 2007. Morphological, electrophysiological, and synaptic properties of corticocallosal pyramidal cells in the neonatal rat neocortex. Cereb Cortex17(9), 2204–2213. [PubMed: 17124287]

Lee D, Lin BJ, Lee AK, 2012. Hippocampal place fields emerge upon single-cell manipulation of excitability during behavior. Science337(6096), 849–853. [PubMed: 22904011]

Luebke JI, Chang YM, 2007. Effects of aging on the electrophysiological properties of layer 5 pyramidal cells in the monkey prefrontal cortex. Neuroscience150(3), 556–562. [PubMed: 17981400]

Luebke JI, Chang YM, Moore TL, Rosene DL, 2004. Normal aging results in decreased synaptic excitation and increased synaptic inhibition of layer 2/3 pyramidal cells in the monkey prefrontal cortex. Neuroscience125(1), 277–288. [PubMed: 15051166]

Luebke JI, Medalla M, Amatrudo JM, Weaver CM, Crimins JL, Hunt B, Hof PR, Peters A, 2015. Age-related changes to layer 3 pyramidal cells in the rhesus monkey visual cortex. Cereb Cortex25(6), 1454–1468. [PubMed: 24323499]

Lur G, Vinck MA, Tang L, Cardin JA, Higley MJ, 2016. Projection-specific visual feature encoding by layer 5 cortical subnetworks. Cell Rep14(11), 2538–2545. [PubMed: 26972011]

Luthi A, Bal T, McCormick DA, 1998. Periodicity of thalamic spindle waves is abolished by ZD7288,a blocker of Ih. J Neurophysiol79(6), 3284–3289. [PubMed: 9636128]

Madison DV, Nicoll RA, 1984. Control of the repetitive discharge of rat CA 1 pyramidal neurones in vitro. J Physiol354, 319–331. [PubMed: 6434729]

Magee JC, 1999. Dendritic lh normalizes temporal summation in hippocampal CA1 neurons. Nat Neurosci2(6), 508–514. [PubMed: 10448214]

Majdi M, Ribeiro-da-Silva A, Cuello AC, 2007. Cognitive impairment and transmitter-specific pre- and postsynaptic changes in the rat cerebral cortex during ageing. Eur J Neurosci26(12), 3583–3596. [PubMed: 18088281]

Matthews EA, Linardakis JM, Disterhoft JF, 2009. The fast and slow afterhyperpolarizations are differentially modulated in hippocampal neurons by aging and learning. J Neurosci29(15), 4750–4755. [PubMed: 19369544]

Mostany R, Anstey JE, Crump KL, Maco B, Knott G, Portera-Cailliau C, 2013. Altered synaptic dynamics during normal brain aging. J Neurosci33(9), 4094–4104. [PubMed: 23447617]

Murchison D, Griffith WH, 1995. Low-voltage activated calcium currents increase in basal forebrain neurons from aged rats. J Neurophysiol74(2), 876–887. [PubMed: 7472390]

Nakahata Y, Yasuda R, 2018. Plasticity of spine structure: Local signaling, translation and cytoskeletal reorganization. Front Synaptic Neurosci10, 29. [PubMed: 30210329]

Oh MM, Simkin D, Disterhoft JF, 2016. Intrinsic hippocampal excitability changes of opposite signs and different origins in CA1 and CA3 pyramidal neurons underlie aging-related cognitive deficits. Front Syst Neurosci10, 52. [PubMed: 27375440]

Oka JI, Jang EK, Hicks TP, 1986. Benzodiazepine receptor involvement in the control of receptive field size and responsiveness in primary somatosensory cortex. Brain Res376(1), 194–198. [PubMed: 3013376]

Oswald MJ, Tantirigama ML, Sonntag I, Hughes SM, Empson RM, 2013. Diversity of layer 5 projection neurons in the mouse motor cortex. Front Cell Neurosci7, 174. [PubMed: 24137110]

Peng YR, Zeng SY, Song HL, Li MY, Yamada MK, Yu X, 2010. Postsynaptic spiking homeostatically induces cell-autonomous regulation of inhibitory inputs via retrograde signaling. J Neurosci30(48), 16220–16231. [PubMed: 21123568]

Peters A, Sethares C, Luebke JI, 2008. Synapses are lost during aging in the primate prefrontal cortex. Neuroscience152(4), 970–981. [PubMed: 18329176]

Petersen CCH, 2019. Sensorimotor processing in the rodent barrel cortex. Nat Rev Neurosci20(9), 533–546. [PubMed: 31367018]

Platkiewicz J, Brette R, 2010. A threshold equation for action potential initiation. PLoS Comput Biol6(7), e1000850. [PubMed: 20628619]

Popescu IR, Le KQ, Palenzuela R, Voglewede R, Mostany R, 2017. Marked bias towards spontaneous synaptic inhibition distinguishes non-adapting from adapting layer 5 pyramidal neurons in the barrel cortex. Sci Rep7(1), 14959. [PubMed: 29097689]

Porciatti V, Fiorentini A, Morrone MC, Burr DC, 1999. The effects of ageing on reaction times to motion onset. Vision Res39(12), 2157–2164. [PubMed: 10343798]

Potier B, Jouvenceau A, Epelbaum J, Dutar P, 2006. Age-related alterations of gabaergic input to CA1 pyramidal neurons and its control by nicotinic acetylcholine receptors in rat hippocampus. Neuroscience142(1), 187–201. [PubMed: 16890374]

Potier B, Rascol O, Jazat F, Lamour Y, Dutar P, 1992. Alterations in the properties of hippocampal pyramidal neurons in the aged rat. Neuroscience48(4), 793–806. [PubMed: 1630625]

Punzi M, Gili T, Petrosini L, Caltagirone C, Spalletta G, Sensi SL, 2017. Modafinil-induced changes in functional connectivity in the cortex and cerebellum of healthy elderly subjects. Front Aging Neurosci9, 85. [PubMed: 28424611]

Radulescu CI, Zabouri N, Barnes SJ, 2019. Age-related decline in homeostatic plasticity. Society for Neuroscience Annual Meeting. Abstract 202.23.

Rock C, Apicella AJ, 2015. Callosal projections drive neuronal-specific responses in the mouse auditory cortex. J Neurosci35(17), 6703–6713. [PubMed: 25926449]

Schwarz JR, Glassmeier G, Cooper EC, Kao TC, Nodera H, Tabuena D, Kaji R, Bostock H, 2006. KCNQ channels mediate IKs, a slow K^+ current regulating excitability in the rat node of ranvier. J Physiol573(Pt 1), 17–34. [PubMed: 16527853]

Seidler RD, Bernard JA, Burutolu TB, Fling BW, Gordon MT, Gwin JT, Kwak Y, Lipps DB, 2010. Motor control and aging: Links to age-related brain structural, functional, and biochemical effects. Neurosci Biobehav Rev34(5), 721–733. [PubMed: 19850077]

Serrien DJ, Swinnen SP, Stelmach GE, 2000. Age-related deterioration of coordinated interlimb behavior. J Gerontol B Psychol Sci Soc Sci55(5), P295–303. [PubMed: 10985294]

Shen H, Liu W, Geng Q, Li H, Lu M, Liang P, Zhang B, Yamoah EN, Lv P, 2018. Age-dependent upregulation of HCN channels in spiral ganglion neurons coincide with hearing loss in mice. Front Aging Neurosci10, 353. [PubMed: 30459593]

Shepherd GM, 2013. Corticostriatal connectivity and its role in disease. Nat Rev Neurosci14(4), 278–291. [PubMed: 23511908]

Shimokata H, Kuzuya F, 1995. Two-point discrimination test of the skin as an index of sensory aging. Gerontology41(5), 267–272. [PubMed: 8537010]

Simkin D, Hattori S, Ybarra N, Musial TF, Buss EW, Richter H, Oh MM, Nicholson DA, Disterhoft JF, 2015. Aging-related hyperexcitability in CA3 pyramidal neurons is mediated by enhanced A-type K^+ channel function and expression. J Neurosci35(38), 13206–13218. [PubMed: 26400949]

Simon NW, LaSarge CL, Montgomery KS, Williams MT, Mendez IA, Setlow B, Bizon JL, 2010. Good things come to those who wait: Attenuated discounting of delayed rewards in aged fischer 344 rats. Neurobiol Aging31(5), 853–862. [PubMed: 18657883]

Spengler F, Godde B, Dinse HR, 1995. Effects of ageing on topographic organization of somatosensory cortex. Neuroreport6(3), 469–473. [PubMed: 7766845]

Spiegel AM, Koh MT, Vogt NM, Rapp PR, Gallagher M, 2013. Hilar interneuron vulnerability distinguishes aged rats with memory impairment. J Comp Neurol521(15), 3508–3523. [PubMed: 23749483]

Spratt PWE, Ben-Shalom R, Keeshen CM, Burke KJ Jr., Clarkson RL, Sanders SJ, Bender KJ, 2019. The autism-associated gene SCN2a contributes to dendritic excitability and synaptic function in the prefrontal cortex. Neuron103(4), 673–685 e675. [PubMed: 31230762]

Sun QQ, Prince DA, Huguenard JR, 2003. Vasoactive intestinal polypeptide and pituitary adenylate cyclase-activating polypeptide activate hyperpolarization-activated cationic current and depolarize thalamocortical neurons in vitro. J Neurosci23(7), 2751–2758. [PubMed: 12684461]

Swinnen SP, 1998. Age-related deficits in motor learning and differences in feedback processing during the production of a bimanual coordination pattern. Cogn Neuropsychol15(5), 439–466. [PubMed: 28657466]

Tang L, Higley MJ, 2020. Layer 5 circuits in V1 differentially control visuomotor behavior. Neuron105(2), 346–354 e345. [PubMed: 31757603]

Tombaugh GC, Rowe WB, Rose GM, 2005. The slow afterhyperpolarization in hippocampal CA1 neurons covaries with spatial learning ability in aged fisher 344 rats. J Neurosci25(10), 2609–2616. [PubMed: 15758171]

Turrigiano GG, 2017. The dialectic of Hebb and homeostasis. Philos Trans R Soc Lond B Biol Sci372(1715).

Turrigiano GG, Leslie KR, Desai NS, Rutherford LC, Nelson SB, 1998. Activity-dependent scaling of quantal amplitude in neocortical neurons. Nature391(6670), 892–896. [PubMed: 9495341]

Voglewede RL, Vandemark KM, Davidson AM, DeWitt AR, Heffler MD, Trimmer EH, Mostany R, 2019. Reduced sensory-evoked structural plasticity in the aging barrel cortex. Neurobiol Aging81, 222–233. [PubMed: 31323444]

White G, Lovinger DM, Weight FF, 1989. Transient low-threshold Ca^{2+} current triggers burst firing through an afterdepolarizing potential in an adult mammalian neuron. Proc Natl Acad Sci U S A86(17), 6802–6806. [PubMed: 2549548]

Wong TP, Marchese G, Casu MA, Ribeiro-da-Silva A, Cuello AC, De Koninck Y, 2000. Loss of presynaptic and postsynaptic structures is accompanied by compensatory increase in action potential-dependent synaptic input to layer v neocortical pyramidal neurons in aged rats. J Neurosci20(22), 8596–8606. [PubMed: 11069968]

Wong TP, Marchese G, Casu MA, Ribeiro-da-Silva A, Cuello AC, De Koninck Y, 2006. Imbalance towards inhibition as a substrate of aging-associated cognitive impairment. Neurosci Lett397(1–2), 64–68. [PubMed: 16378682]

Wu T, Hallett M, 2005. The influence of normal human ageing on automatic movements. J Physiol562(Pt 2), 605–615. [PubMed: 15513939]

Ye Z, Mostajo-Radji MA, Brown JR, Rouaux C, Tomassy GS, Hensch TK, Arlotta P, 2015. Instructing perisomatic inhibition by direct lineage reprogramming of neocortical projection neurons. Neuron88(3), 475–483. [PubMed: 26539889]

Yoder WM, Gaynor LS, Burke SN, Setlow B, Smith DW, Bizon JL, 2017. Interaction between age and perceptual similarity in olfactory discrimination learning in F344 rats: Relationships with spatial learning. Neurobiol Aging53, 122–137. [PubMed: 28259065]

Highlights

- Aging increases excitability of principal neurons in mouse somatosensory cortex.
- Aging also decreases the synaptic inhibition of these neurons.
- Increased excitability & decreased synaptic inhibition suggests deficient homeostasis.
- Two pyramidal neuron types in layer 5 have different hyperexcitability mechanisms.
- By knowing the type-specific aging mechanisms we can understand effects of treatments.

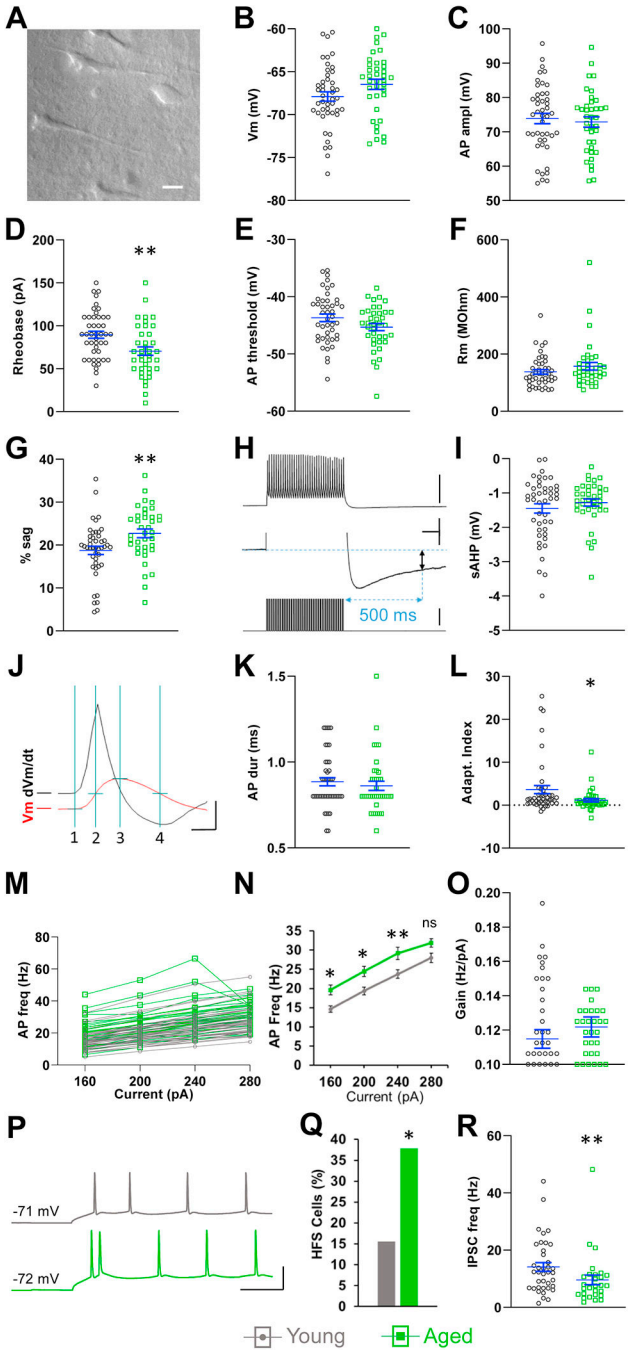

Fig. 1.

Effects of age on L5 pyramidal neurons of S1BF. (A) Representative bright field photograph of S1BF L5 in an aged mouse brain slice used for patch clamp recordings in this study. (B,C) Two indicators of cellular health, resting membrane potential (B), and AP amplitude (C), were not different in young and aged neurons. (D) Rheobase was significantly reduced in aged neurons. (E,F) AP threshold and input resistance were not different in young and aged neurons. (G) Sag was increased in aged neurons. (H) The sAHP (two-headed black arrow, middle trace) is the difference between Vm immediately before and 500 ms after a

70 Hz, 500 ms train of intracellular current injections (lower trace), each injection eliciting an AP (top trace). The middle trace is the top trace shown at expanded vertical scale. (I) The sAHP was not different in young and aged neurons. (J) Quantification of APs (red trace, Vm): AP duration was measured at half-amplitude (line 2 to line 4). Amplitude (line 1 to line 3) was measured from threshold to peak. Threshold was measured at the time point when the first derivative of the membrane potential (dVm/dt, black trace) reached 10 mV/ms. (K) AP duration was not different in young and aged neurons. (L) Aged neurons displayed reduced spike frequency adaptation. Negative AI indicates spike frequency acceleration (Guan et al., 2018; Popescu et al., 2017). (M,N) The *f-I* relationship indicates increased excitability in aged neurons in response to current steps. (O) The slope (gain) of the linear segment of the *f-I* relationship (160 pA to 240 pA) was not affected by age. (P) Representative HFS occurring in the initial 60 ms of 280 pA step injection in an aged neuron (green, lower trace). First interspike interval = 6.3 ms. The first interspike interval in the equivalent recording from a young neuron (gray, top trace) is 27 ms. (Q) The prevalence of cells engaged in HFS was higher in aged neurons. (R) Aged neurons show a reduced sIPSC frequency. A-N, $n = 45$ cells from 30 young mice, 38 cells from 22 aged mice. O-Q, $n = 45$ cells from 30 young mice, 37 cells from 22 aged mice. R, $n = 38$ cells from 27 young mice, 28 cells from 19 aged mice. Horizontal lines with error bars in scatter plots indicate the mean and SE. * $p < 0.05$, ** $p < 0.01$. Scale bars. A: 20 μm. H: top 60 mV, middle 2 mV, 100 ms, bottom 350 pA. J: 80 mV, 0.4 ms. P: 50 mV, 50 ms.

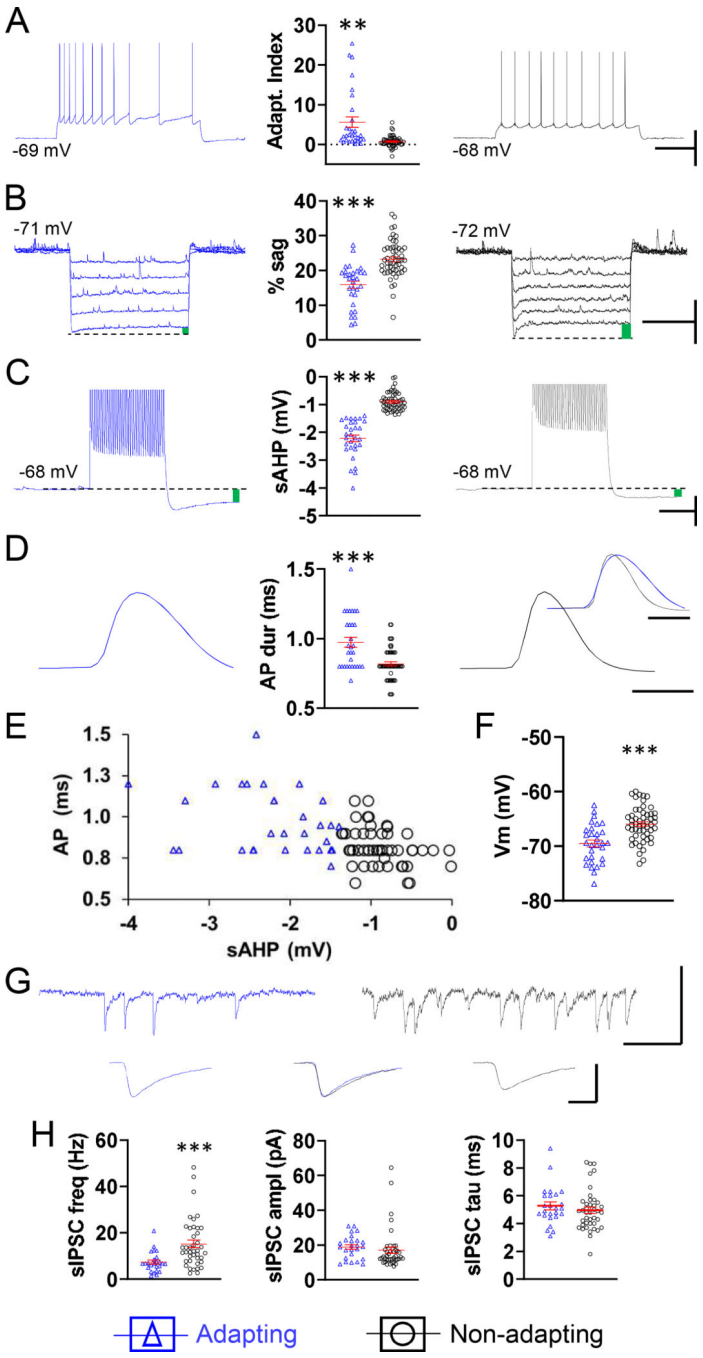

Fig. 2.

The two populations of L5 pyramidal neurons determined by cluster analysis, adapting and non-adapting, have contrasting intrinsic properties and different IPSC frequencies. Representative examples of spike frequency adaptation (A), sag, indicated by green bar (B), sAHP, average of 5 traces, indicated by green bar (C), and spike duration, average of 3 traces, scaled for amplitude (D), all from one neuron in the adapting group (left, blue) and all from one neuron in the non-adapting group (right, black). Respective summary graphs are found between traces. (E) Plot of AP duration at half-amplitude as a function of sAHP

illustrating the clustering of neurons into a group with longer duration APs and larger sAHP (blue triangles) and a group with shorter duration APs and smaller sAHP (black circles). (F) Summary graph of resting membrane potential for neurons in the adapting and non-adapting groups. (G) Top, representative traces illustrating the sIPSC frequency and amplitude in the neuron from the adapting group (left, blue) and the neuron from the non-adapting group (right, black). Below, averaged traces of 50 consecutive, non-summating sIPSCs from each of the two cells above. Below, middle, the flanking traces were amplitude-scaled and superimposed in order to compare kinetics. (H) Respective summary graphs of sIPSC frequency, amplitude, and decay time (tau). A-F, $n = 30$ adapting cells from 25 mice (left), 53 non-adapting cells from 40 mice (right). H, $n = 25$ adapting cells from 20 mice (left), 41 non-adapting cells from 36 mice (right). Of ten GFP+ neurons recorded, one belonged to the adapting category, nine to the non-adapting category. Horizontal lines with error bars in scatter plots indicate the mean and SE. ** $p < 0.01$, *** $p < 0.001$. Scale bars. A: 40 mV, 500 ms. B: 10 mV, 1 s. C: 10 mV, 250 ms. D: 1 ms. G: top 50 pA, 100 ms, bottom, 20 pA, 2 ms.

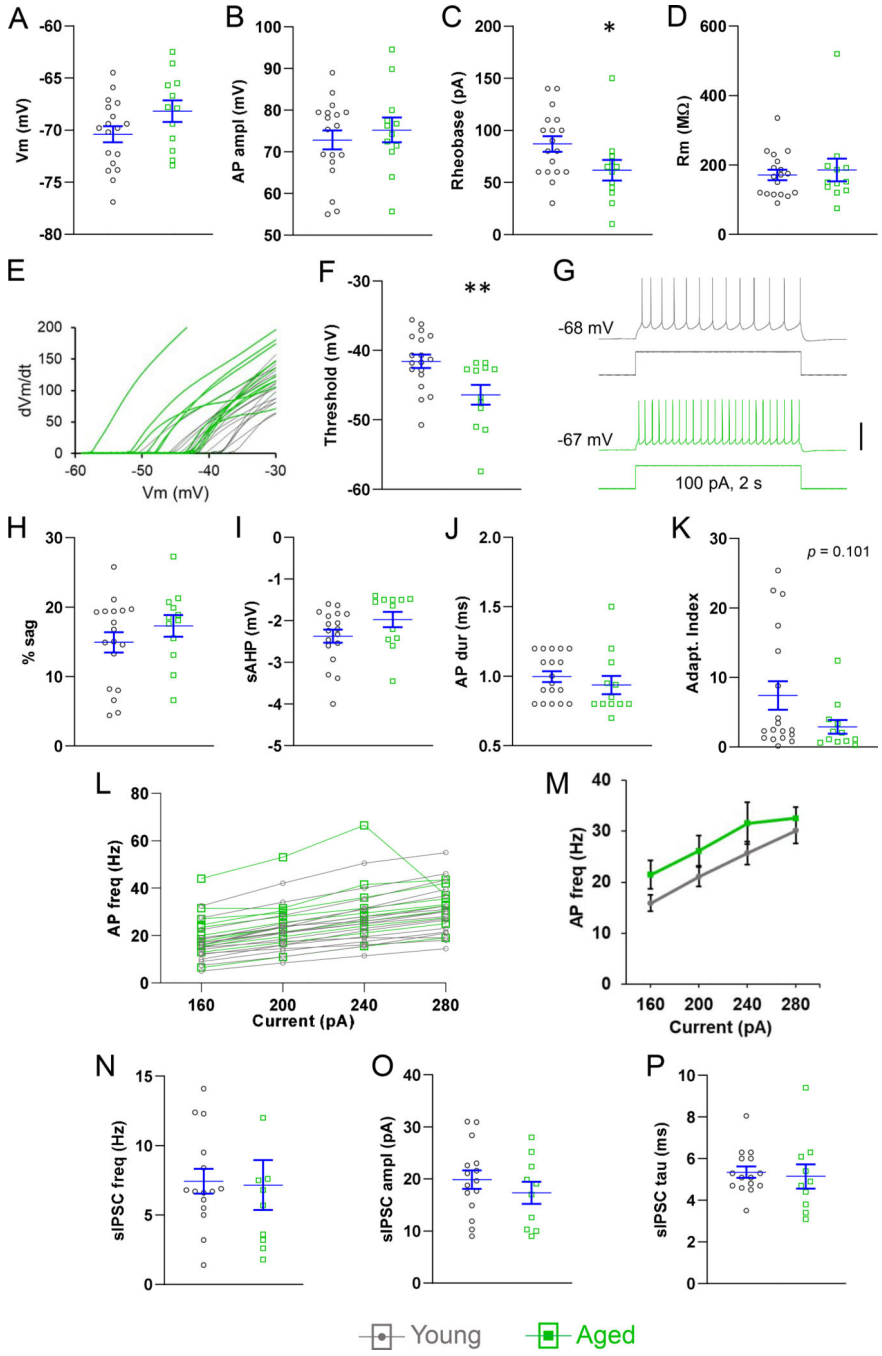

Fig. 3.

Effects of age on adapting pyramidal neurons. Resting potential (A), and AP amplitude (B) were not different in young and aged neurons. (C) Rheobase was lower in aged neurons. (D) Input resistance was not affected by age. (E) Plot of first derivative of the AP voltage (Y-axis) and the AP voltage (X-axis) from each neuron in the adapting group, illustrating the higher prevalence of more negative thresholds in the aged neurons (green). (F) AP threshold was reduced in aged neurons. (G) Representative recordings illustrating an aged neuron that fired more APs (lower trace, green) than a young neuron (top, gray) in response to

near-rheobase current steps (data summary in Results). (H-J) Sag, sAHP, and AP duration were not different in the two age groups. (K) Aged neurons displayed a trend towards reduced spike frequency adaptation. (L,M) The *f-I* relationship did not reveal a significant change in excitability between the age groups. (N-P) IPSC frequency, amplitude, and decay time were not affected by age. A-M, $n = 18$ neurons from 16 young mice, 12 neurons from 9 aged mice. N-P, $n = 15$ neurons from 13 young mice, 10 neurons from 7 aged mice. Horizontal lines with error bars indicate the mean and SE. * $p < 0.05$, ** $p < 0.01$. Scale bar: G, 50 mV.

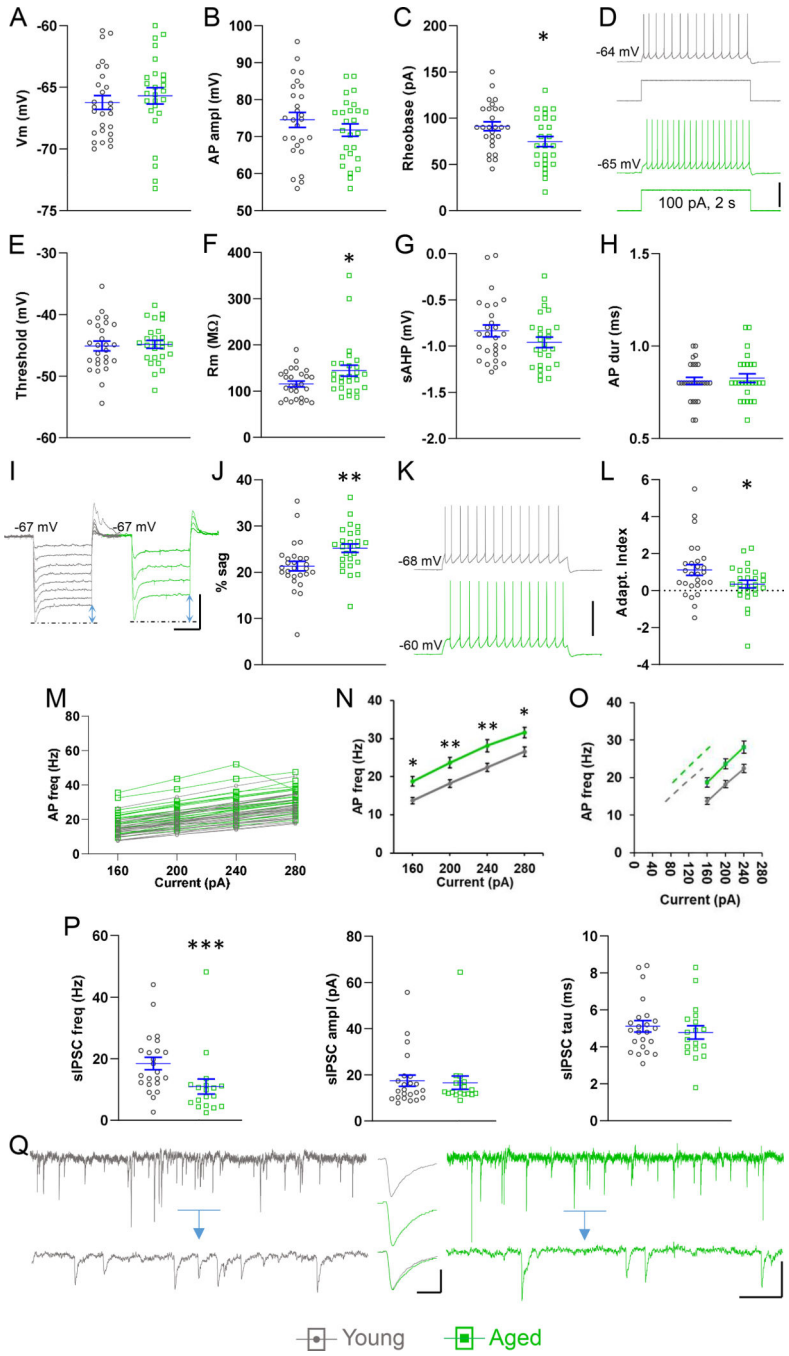

Fig. 4.

Effects of age on non-adapting pyramidal neurons. (A,B) Resting potential (A) and AP amplitude (B) were not different in young and aged neurons. (C) Rheobase was lower in aged neurons. (D) Representative recordings illustrating higher AP frequency in an aged neuron (lower trace, green) than in a young neuron (top, gray) in response to a 2 s near-rheobase current step (data summary in Results). (E) AP threshold was not affected by age. (F) Input resistance was higher in aged neurons. (G,H) sAHP and AP duration were not different in the two age groups. (I,J) Sag, indicated by blue arrows, was increased in aged

neurons. (K) Representative traces illustrating subtle, higher spike frequency adaptation in a young neuron (gray, upper) compared to an aged neuron (green, lower), at 7 Hz firing in response to 2 s current injection. (L) Spike frequency adaptation was significantly reduced in aged neurons. (M,N) The *f-I* relationship indicated increased excitability in aged neurons in response to current steps. (O) Subtracting the mean rheobase from the X-values in the linear range of the *f-I* function does not result in superimposed plots (solid gray – young, solid green – aged, dashed gray – young after rheobase subtraction, dashed green – aged after rheobase subtraction). (P) Mean sIPSC frequency was significantly lower in neurons from aged mice, but amplitude and decay time were not different in the two age groups. (Q) Left, gray: representative trace from a non-adapting neuron from a young mouse, showing IPSCs as inward currents at a holding potential of −70 mV. The detail lower trace is from the blue bar-indicated period, expanded. Right, green: same but from an aged mouse, illustrating the lower IPSC frequency. Insert, gray (top): average trace of 50 consecutive, non-summating sIPSCs from the young neuron. Insert, green (middle): same as top, from the aged neuron. Insert (bottom): the average traces from the young neuron and the aged neuron were height normalized and superimposed to compare kinetics. A-O, $n = 27$ neurons from 22 young mice, 26 neurons from 18 aged mice. P,Q, $n = 23$ neurons from 20 young mice, 18 neurons from 16 aged mice. Horizontal lines with error bars indicate the mean and SE. * $p < 0.05$, ** $p < 0.01$, *** $p < 0.001$. Scale bars: (D) 40 mV, (I) 10 mV, 500 ms, (K) 40 mV, (Q) 20 pA, 500 ms, 60 ms, inset 10 pA, 4 ms.